Available online at www.sciencedirect.com
SCIENCE DIRECT®
Mechatronics 15 (2005) 487–503
MECHATRONICS

Slewing and vibration control of a single-link flexible manipulator by positive position feedback (PPF)

Jinjun Shan [a,*], Hong-Tao Liu [a], Dong Sun [b]

[a] The Institute for Aerospace Studies, University of Toronto, 4925 Dufferin Street, Toronto, ON, Canada M3H 5T6
[b] Department of Manufacturing Engineering and Engineering Management, City University of Hong Kong, 83 Tat Chee Avenue, Kowloon, Hong Kong

Abstract

Positive position feedback (PPF) is an effective vibration control technique for smart actuators and has been studied in recent years. In this paper, PPF controller is analyzed and applied to the PZT actuators for suppressing multi-mode vibrations while slewing the single-link flexible manipulator. Both set-point and trajectory tracking control are considered. Moreover, PPF is compared with L-type velocity feedback for PZT actuators to verify the characteristic of anti-spillover of PPF. The hardware experiments verified the proposed method.

Keywords: Single-link flexible manipulator; Positive position feedback (PPF); Vibration control; Slewing

1. Introduction

Increasing demand for high-speed performance and low energy consumption of robotic systems coupled with needs of space applications have necessitated the

* Corresponding author. Tel.: +1 416 667 7855; fax: +1 416 667 7799.
E-mail address: shan@utias.utoronto.ca (J. Shan).

0957-4158/$ - see front matter © 2004 Elsevier Ltd. All rights reserved.
doi:10.1016/j.mechatronics.2004.10.003

design of light-weight manipulators. These light manipulators may possess significant flexibility that must be taken into consideration in the control design [1]. Considerable work has been carried out in the control of flexible manipulators by various researchers [2–4].

With recent developments in sensor/actuator technologies, many researchers have concentrated on control methods for suppressing vibrations of flexible structures using smart materials such as Shape Memory Alloys (SMA) [5], Magnetorheological (MR) materials [6], Electrorheological (ER) materials [7], and Piezoelectric transducers [8–16] etc.

Piezoelectric actuators convert electrical energy into mechanical energy via the inverse piezoelectric effect: a piezoelectric material subjected to an external electrical field extends or contracts depending on the orientation of the applied field and the internal polarization. Alternatively, piezoelectric sensors generate an electrical charge in response to a mechanical deformation via the direct piezoelectric effect [17]. Piezoelectric materials have been applied in structural vibration control as well as in structure acoustics because of their advantages of fast response, large force output and the fact that they generate no magnetic field in the conversion of electrical energy into mechanical motion. The piezoelectric transducers are usually constructed from two types of materials: one is polyvinylidene fluoride (PVDF) [8,9], another one is lead zirconium titanate (PZT). In general, PZT is used as actuator and PVDF as sensor because the piezoelectric constant of PVDF is roughly 10 times greater than that of PZT. In this paper, we use PZT as the actuators for vibration suppression.

Many control strategies have been applied to PZT actuators, such as velocity feedback [16], neural networks [18], genetic algorithms [19], adaptive control [20], fuzzy control [21], and so on.

Positive position feedback (PPF) was introduced by Goh and Caughey in 1985 [22] to control vibration of large flexible space structures. It was applied by feeding the structural position coordinate directly to the compensator and the product of the compensator and a scalar gain positively back to the structure. An autonomous control technique was developed to design the optimal feedback compensator using on-line Pole-Zero identification in [23]. McEver and Leo [24] pointed out that a PPF controller can be formulated as an output feedback controller and control design algorithms for output feedback systems can be used to design PPF controller. PPF control was implemented for single-mode vibration suppression and for multi-mode vibration suppression, and the robustness of PPF controller to uncertainty in frequency was studied in [25]. PPF controller has several distinguished advantages as compared to the widely used velocity feedback control laws:

(1) It is insensitive to spillover, where contributions from unmodeled modes affect the control of the modes of interest. As a second-order low-pass filter, a PPF controller rolls off quickly at high frequencies.
(2) It is not destabilized by finite actuator dynamics and stability may be assured by consideration of the structure's stiffness properties only.

(3) It can offer quick damping for a particular mode provided that the modal characteristics are well known.
(4) PPF is easy to implement.

For these advantages, PPF controller has been applied to many flexible systems with bonded PZT actuators to achieve active damping.

The remainder of this paper is organized as follows. Section 2 discusses and analyzes the PPF adopted in this paper. It is shown that a big damping ratio of the compensator can make it more robust to the uncertainty in modeling frequency. In Section 3, a single-link flexible manipulator with bonded PZT actuators is modeled according to assumed modes method. Section 4 describes the experimental work. The experimental setup is introduced first and its natural characteristics are measured experimentally. Based on these parameters, the PPF controllers for the first two vibration modes are designed to control the PZT actuators while a traditional PD feedback law is applied to control the hub motion. The experimental results are discussed in this section too. Finally, the conclusions are given in Section 5.

2. Positive position feedback

Fig. 1 demonstrates the control scheme of PPF method. In the single-degree-of-freedom form, PPF introduces a second-order auxiliary system, which is forced by the position response of the structure. The position response of the auxiliary system is then fed back to give the force input to the structure. The controller is essentially a second-order compensator, and the stability of closed-loop system can be guaranteed only by adjusting the relationship between the natural frequency of the structure and the feedback gain. The transfer function of the controller rolls off quickly at high frequencies making the approach well suited to controlling the lower frequency modes of the structure with well separated modes, as the controller is insensitive to the unmodeled high frequency dynamics. One disadvantage of applying a PPF controller is that the control makes the structure more flexible, which can lead to larger steady state errors [23].

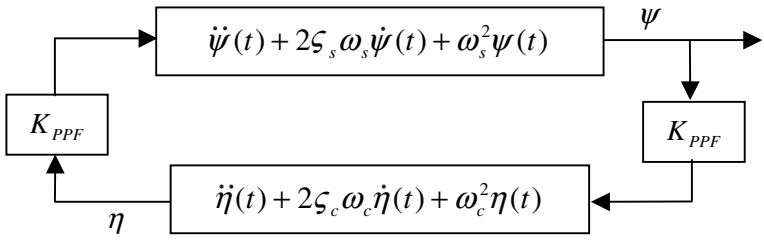

Fig. 1. Positive position feedback block diagram.

The equations describing PPF technique are given as

$$\ddot{\psi}(t) + 2\varsigma_s\omega_s\dot{\psi}(t) + \omega_s^2\psi(t) = K_{PPF}\eta \tag{1}$$

$$\ddot{\eta}(t) + 2\varsigma_c\omega_c\dot{\eta}(t) + \omega_c^2\eta(t) = K_{PPF}\psi \tag{2}$$

where ψ is the displacement of the structure; ς_s and ω_s are the damping ratio and the natural frequency of the structure; η is the displacement of the compensator; ς_c and ω_c are the damping ratio and frequency of the compensator; K_{PPF} is the feedback gain.

Writing the above equations into state-space form, we have

$$\begin{bmatrix} \ddot{\psi} \\ \ddot{\eta} \end{bmatrix} + \begin{bmatrix} 2\varsigma_s\omega_s & 0 \\ 0 & 2\varsigma_c\omega_c \end{bmatrix} \cdot \begin{bmatrix} \dot{\psi} \\ \dot{\eta} \end{bmatrix} + \begin{bmatrix} \omega_s^2 & -K_{PPF} \\ -K_{PPF} & \omega_c^2 \end{bmatrix} \cdot \begin{bmatrix} \psi \\ \eta \end{bmatrix} = \begin{bmatrix} 0 \\ 0 \end{bmatrix} \tag{3}$$

The closed-loop system in (3) is stable if the stiffness matrix is positive definite, i.e. the eigenvalues are all positive. This condition can be satisfied if and only if

$$K_{PPF} < \omega_s \cdot \omega_c \tag{4}$$

When the structural modal frequency is much lower than the compensator natural frequency, the PPF compensator in this case results in the stiffness term being decreased, which is called *active flexibility*.

When the compensator and the structure have the same natural frequency, the PPF compensator in this case results in an increase in the damping term, which is called *active damping*.

When the structure frequency is much greater than that of the compensator, the PPF compensator in this case results in an increase in the stiffness term, which is called *active stiffness*.

Obviously, to achieve maximum damping, ω_c should be closely matched to ω_s.

The closed-loop transfer function $G(s)$ of the whole system is

$$\begin{aligned} G(s) = {} & [K_{PPF} \cdot (s^2 + 2\varsigma_c\omega_c + \omega_c^2)]/s^4 + 2(\varsigma_s\omega_s + \varsigma_c\omega_c)s^3 + (\omega_s^2 + \omega_c^2 + 4\varsigma_c\omega_c\varsigma_s\omega_s)s^2 \\ & + 2\omega_s\omega_c(\varsigma_s\omega_c + \varsigma_c\omega_s)s + (\omega_s^2\omega_c^2 + K_{PPF}^2) \end{aligned} \tag{5}$$

Fig. 2 shows two bode diagrams for $\varsigma_c = 0.15$ and $\varsigma_c = 0.60$, respectively. The other parameters used for plotting are $\omega_s = \omega_c = \pi$ rad/s, $\varsigma_s = 0.2$, $K_{PPF} = 8$. It can be seen that there is obvious difference between the slopes of the phase angle. The difference implies that the larger damping ratio ς_c can ensure a larger region of active damping and thus will increase the robustness of the compensator with respect to uncertain modal frequencies [25].

Fig. 3 shows the simulation result with various damping ratios of PPF compensator. The simulation parameters are: $\omega_s = \omega_c = 6\pi$ rad/s, $\varsigma_s = 0.05$, $K_{PPF} = 317.8$, $\psi(0) = 1$ mm. Simulation shows that the better vibration suppression can be achieved by increasing the damping ratio of the PPF compensator while keeping the other parameters invariant.

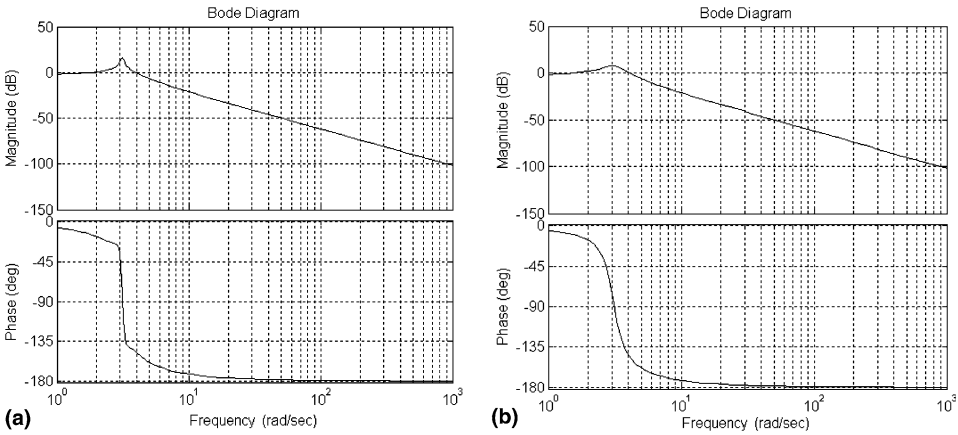

Fig. 2. Bode diagrams of PPF controller with various damping ratios: (a) Bode diagram for $\varsigma_c = 0.15$ and (b) Bode diagram for $\varsigma_c = 0.60$.

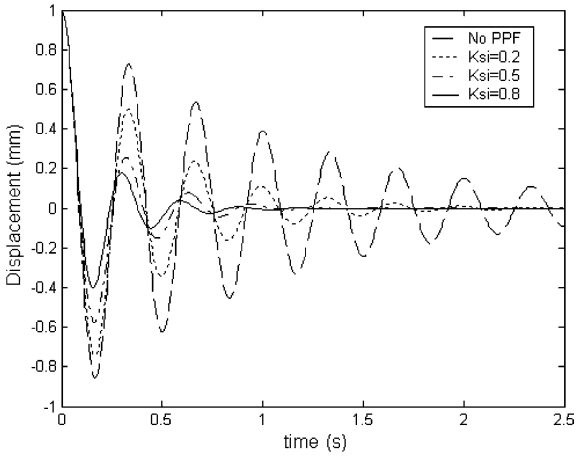

Fig. 3. Simulation results of PPF controller with various damping ratios.

3. Dynamic modeling

A single-link flexible manipulator with tip mass and bonded PZT actuators is modeled as a uniform cantilever beam that can rotate about the Z-axis perpendicular to the paper, as shown in Fig. 4. The control system includes attitude control torque acting on the hub for rigid motion, and n piezoelectric (PZT) actuators bonded on the beam's surface for vibration damping. Each PZT actuator is uniformly designed and its location is represented by coordinates a_{i1} and a_{i2} ($i = 1, \ldots, n$). By applying control voltage, the PZT actuator generates a shear force that can be used to damp the vibration. For system modeling, the following assumptions are made: (1) the

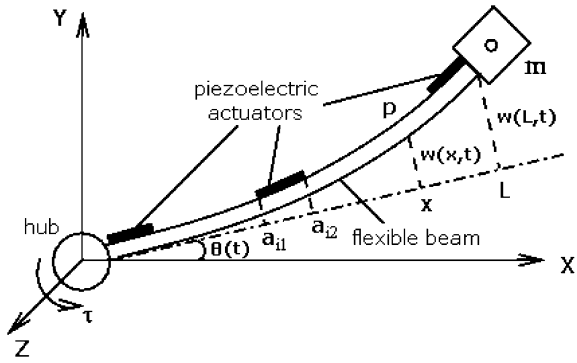

Fig. 4. A single-link flexible manipulator with bonded PZT actuators.

beam is considered to be an Euler–Bernoulli beam and the axial deformation is neglected; (2) PZT actuators are perfectly bonded to the beam; (3) each PZT actuator has constant thickness and the same width as the beam; and (4) the gravitational effect and the hub dynamics are neglected for simplicity.

Define $w(x,t)$ as the deflection of the beam at point x (see Fig. 4), where t denotes time and $x \in [0, L]$ the beam coordinate. The deflection $w(x,t)$ can be represented using the assumed mode:

$$w(x,t) = \sum_{k=1}^{m} \phi_k(x) q_k(t) = \phi(x) q(t) \tag{6}$$

where $\phi_k(x)$ is the shape function, $q_k(t)$ denotes the generalized modal coordinate, and k represents the mode number ($k = 1, \ldots, m$).

Applying Lagrange's theory, the completed system equation can be obtained as follows:

$$\underbrace{\begin{bmatrix} m_{\theta\theta} & m_{\theta q} \\ m_{\theta q}^{\mathrm{T}} & m_{qq} \end{bmatrix}}_{M(q)} \begin{bmatrix} \ddot{\theta} \\ \ddot{q} \end{bmatrix} + \underbrace{\begin{bmatrix} \dot{q}^{\mathrm{T}} m_{qq} q & \dot{\theta} q^{\mathrm{T}} m_{qq} \\ -\dot{\theta} m_{qq} q & 0 \end{bmatrix}}_{C(\dot{\theta}, q, \dot{q})} \begin{bmatrix} \dot{\theta} \\ \dot{q} \end{bmatrix} + \begin{bmatrix} 0 \\ K_q q \end{bmatrix} = \begin{bmatrix} u(t) + \sum_{i=1}^{n} c V_i(t) \\ \sum_{i=1}^{n} c V_i(t) \end{bmatrix} \tag{7}$$

where θ is the hub angle with respect to the inertial X-axis (see Fig. 3); $M(q)$ and $C(\dot{\theta}, q, \dot{q})$ denote the system inertia and nonlinear effects, respectively; K_q is the stiffness matrix of this flexible system; $u(t)$ is the control input; $V_i(t)$ is a uniform control voltage applied to the ith PZT actuator and $cV_i(t)$ is a bending moment generated by the ith PZT actuator. For detailed derivation and expression, please see [16].

It can be seen from (7) that the rigid motion and the flexible vibration are coupled via matrices $M(q)$ and $C(\dot{\theta}, q, \dot{q})$. Moreover, the matrix $C(\dot{\theta}, q, \dot{q})$ shows that the nonlinearity is related to the slewing rate, $\dot{\theta}$, and the flexible vibration, q and $\dot{q}$. The faster the slewing and the larger the vibration amplitude, the stronger the nonlinearity will be.

4. Experiments

Fig. 5 shows the scheme of the experimental setup used to verify the approach proposed in this paper. This device consists of a flexible aluminum beam ($0.5\,m \times 0.03\,m \times 0.003\,m$) and a SANYO servo AC motor with a reduction gear 1:25. The lightweight flexible beam is clamped at the shaft of the motor through a coupling and is limited to rotate only on the horizontal plane, so the effect of gravity can be ignored. The tip deflection of the link is measured by a system consists of a laser diode, which locates at the hub, and a PSD (Position Sensitive Detector) installed at the tip of the flexible beam. The measurement range of the PSD is $\pm 8\,mm$. A built-in incremental encoder is used to calculate the rotating angle of the hub. The encoder resolution is 0.0072° per pulse. A three-axis quadrature encoder and counter card, PCL-833, is used to count the encoder pulses. The analogue signal of the PSD is converted into digital data through a PCL-818HD A/D card. The control voltages for the motor and the PZT actuators (ACX QuickPack-QP40N, see Table 1 for detailed properties) are sent to the servo amplifier and the ACX amplifier (35.6×), respectively, through a PCL-727 D/A card.

Although it is known that the best location for vibration suppression of the clamped-free beam using one actuator is near the root of the beam [16], in our experiment, the actuator was placed near the tip to nearly collocate the PZT actuator with the PSD sensor. Fig. 6 shows a photograph of this configuration.

To identify the mode characteristic of the flexible beam, we conducted the following steps: (1) Applying a bang–bang voltage command to drive the motor; (2) Measuring the deflection at the tip by PSD; and (3) Implementing the fast fourier transform (FFT) to achieve the frequency-domain information. Fig. 7 shows the measured deflection curve using PSD and the corresponding FFT result. It can be seen that the first two modes play a main role in the vibration of the beam. The frequencies of the first two modes are 25.1529 rad/s and 50.2655 rad/s, respectively. For

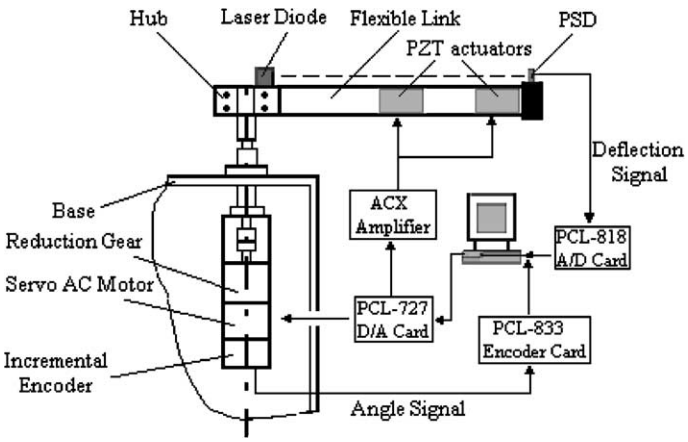

Fig. 5. Scheme of the single-link flexible manipulator experimental setup.

Table 1
Properties of PZT actuators

Property	Value
Size of PZT actuators, m ($\times 10^{-3}$)	$101.6 \times 25.4 \times 0.762$
Weight, kg ($\times 10^{-3}$)	9.639
Capacitance, F ($\times 10^{-6}$)	0.26
Full scale voltage range, V	± 200
Direct charge coefficient, d_{33}, C/N	350×10^{-12}
Transverse charge coefficient, d_{31}, C/N	-179×10^{-12}
Direct voltage coefficient, g_{33}, Vm/N	24.2×10^{-3}
Transverse voltage coefficient, g_{31}, Vm/N	-11.0×10^{-3}

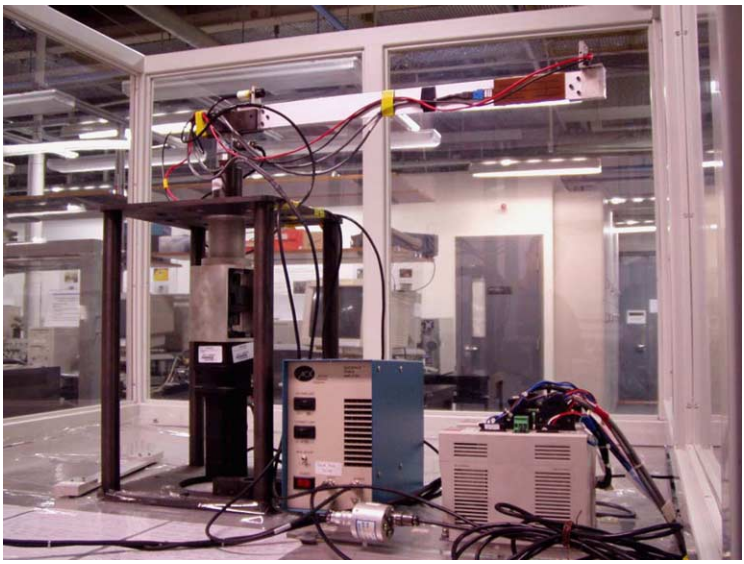

Fig. 6. Photograph of the experimental setup.

the damping ratio, we calculated it on the basis of decay characteristic of the measured vibration signal. The mode parameters of the flexible beam are listed in Table 2. It should be noted that the frequencies and damping ratios of the flexible beam with PD feedback controller will be different from those values obtained by applying the open-loop bang–bang commands. These differences are small for our flexible system because it has a large reduction gear and a light flexible beam. Thus, we still use the measured frequencies and damping ratios in Table 2.

In the following PPF experiments, several third-order bandpass Butterworth digital filters are used to pre-filter the measured tip deflection data. Two filters with passband frequency of 0.5–6.0 Hz (3.14–37.7 rad/s) and 6.0–10.0 Hz (37.7–62.8 rad/s) are employed to get the values of the first and the second vibration modes, respec-

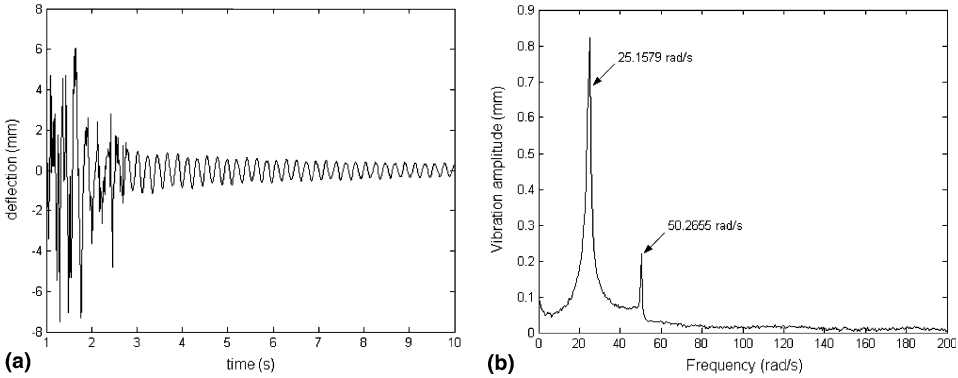

Fig. 7. Tip deflection of the flexible beam: (a) PSD measurement and (b) FFT of the measurement.

Table 2
Mode parameters of the experimental flexible manipulator

Mode	1	2
Frequency, rad/s	25.1529	50.2655
Damping ratio	0.0045	0.004

tively. Another filter with passband frequency of 0.5–20.0 Hz (3.14–125.6 rad/s) is adopted to obtain the final vibration result for reduction of the low-frequency offset and the high-frequency noise.

4.1. Controller design

In this section, we first develop a PD feedback control law for the hub angle motion to rotate the single-link flexible manipulator. Secondly, the parameters of the PPF controllers for the first and the second vibration modes are chosen based on the measured frequencies and damping ratios, the stability requirement and the robustness requirement.

The following PD feedback controller is designed to drive the motor:

$$\tau(t) = -K_{\mathrm{P}}e(t) - K_{\mathrm{D}}\dot{e}(t) \tag{8}$$

where $e(t) = \theta(t) - \theta_{\mathrm{d}}$, $\dot{e}(t) = \dot{\theta}(t) - \dot{\theta}_{\mathrm{d}}$ are the position error and the velocity error, respectively; θ_{d} is the desired slewing angle trajectory for rigid motion; K_P and K_D are proportional and derivative gains.

To compensate for the motor friction, the practical control torque, τ_{p}, was defined by

$$\tau_{\mathrm{p}}(t) = \tau(t) + 0.002\dot{\theta}(t) + 0.005\,\mathrm{sgn}(\dot{\theta}(t)) \tag{9}$$

where $\tau(t)$ is the same as in (8), and the remaining two terms denote the feedforward compensations of the viscous and coulomb frictions. The compensation coefficients are selected experimentally.

Two PPF controllers for the first and the second modes are designed according to the measured natural frequencies of the flexible beam. The two PPF controllers are given in (10), for the first mode, and (11), for the second mode.

$$\ddot{\eta}_1(t) + 2\varsigma_{c1}\omega_{c1}\dot{\eta}_1(t) + \omega_{c1}^2\eta_1(t) = K_1\psi_1 \tag{10}$$

$$\ddot{\eta}_2(t) + 2\varsigma_{c2}\omega_{c2}\dot{\eta}_2(t) + \omega_{c2}^2\eta_2(t) = K_2\psi_2 \tag{11}$$

where subscripts 1 and 2 represent the parameters relative to the first and the second vibration modes, respectively; ψ are the filtered value of PSD measurement with adopted bandpass Butterworth filters; the frequencies of the PPF controllers, ω_{c1} and ω_{c2}, are chosen to be the same as those measured values of the flexible beam in Table 2; the damping ratios of the PPF controllers, ς_{c1} and ς_{c2}, are chosen to be large enough for robustness [25]; η are the outputs of PPF controllers; K are the feedback gains of PPF controllers and are chosen with consideration of stability requirement in (4). The complete parameters for these two PPF controllers are listed in Table 3.

Finally, the outputs of the PPF controllers are combined to produce control input of the PZT actuators multiplied by feedback gains K_1 and K_2, i.e. $U = K_1\eta_1 + K_2\eta_2$.

4.2. Experimental results

Experiments are conducted to rotate the hub angle 40° while suppressing flexible vibration using PD controller and multi-mode PPF controller. Two slewing cases have been taken into account in experiments: (1) set-point control (the reference input angle of the hub is a step command), and (2) trajectory tracking control (the reference input angle of the hub is a smoothed polynomial command). A quintic polynomial in (12) is used to generate the reference trajectory for hub motion. This polynomial can specify the position, velocity, and acceleration at both boundaries.

$$\theta(t) = \sum_{i=0}^{5} \alpha_i \cdot t^i \tag{12}$$

Table 3
Values of the PPF controllers

Parameters	Value
Frequency of PPF Controller 1, ω_{c1}, rad/s	25.1529
Frequency of PPF Controller 2, ω_{c2}, rad/s	50.2655
Damping of PPF Controller 1, ς_{c1}	0.707
Damping of PPF Controller 2, ς_{c2}	0.707
Feedback Gain 1, K_1	15.0
Feedback Gain 2, K_2	50.0

From the six constraints on the position, velocity, and acceleration of the initial and final time, the coefficients α_i can be determined. In our experiments, we design the point-to-point reference trajectory to rotate the hub from 0° to 40° in 2 s. Thus, the coefficients α_0–α_5 are $(0, 0, 0, 50.0, -37.5, 7.5)$. For each case, the feedback gains of the PD controller (8) are determined experimentally to achieve a good-compromise hub-angle response in terms of the overshoot, rise time, and settling time while considering the measurement range of the PSD. Finally, the gains for set-point control (13) and trajectory tracking control (14) are:

$$K_P = 0.05, \quad K_D = 0.02 \tag{13}$$

$$K_P = 0.30, \quad K_D = 0.12 \tag{14}$$

and the sampling frequency was set to 10 ms (100 Hz).

The experimental results are plotted in Figs. 8–11. Among them, Figs. 8 and 9 are the results of set-point control and Figs. 10 and 11 are the results of trajectory tracking control, the subsequent figure (a) shows the hub angle motion of the flexible manipulator, (b) shows the tip deflection measured using PSD, and (c) is the FFT result of the PSD measurement.

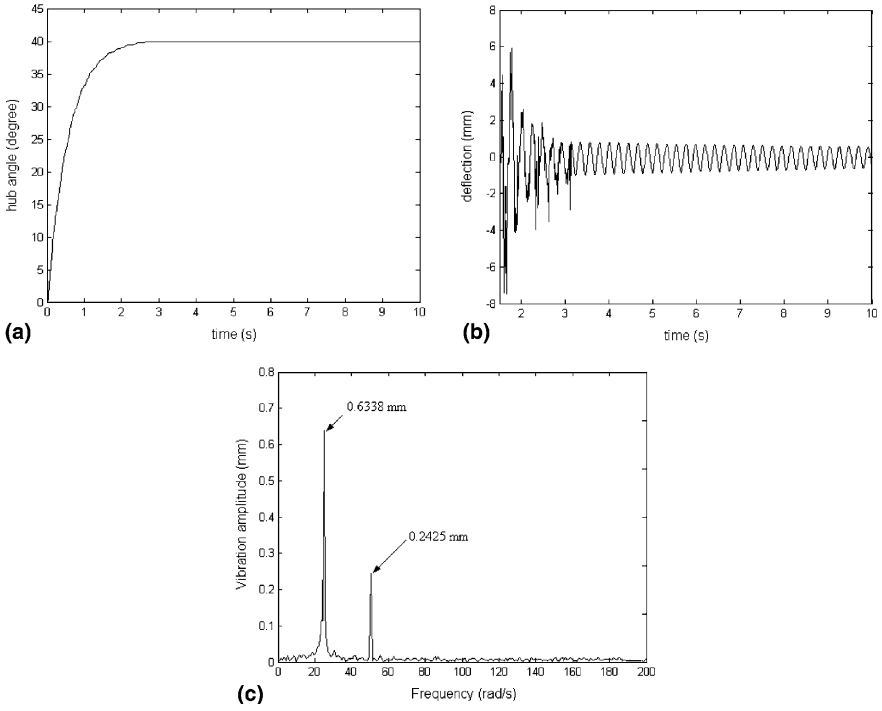

Fig. 8. Set-point control experiment result without PPF control: (a) Hub angle motion, (b) PSD measurement and (c) FFT of PSD measurement.

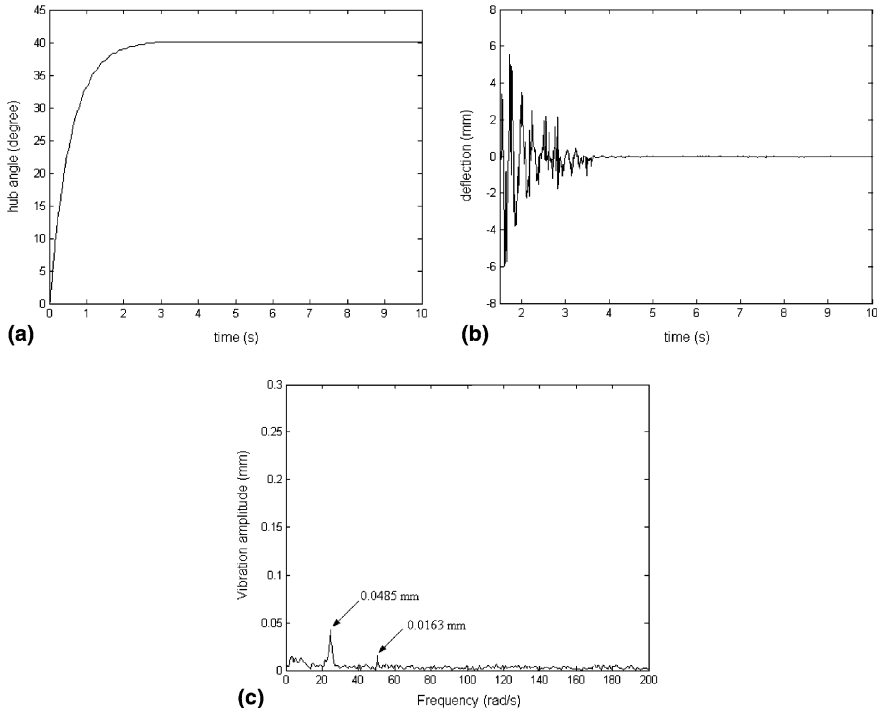

Fig. 9. Set-point control experiment result with PPF control: (a) Hub angle motion, (b) PSD measurement and (c) FFT of PSD measurement.

Because the PPF controller does not work, after the slewing, the vibration amplitudes for the first two modes are large: 0.6338 mm, 0.2425 mm for the set-point control in Fig. 8 and 0.4994 mm, 0.1928 mm for the trajectory tracking control in Fig. 10. Comparing with these results, the tip deflections are effectively suppressed when the multi-mode PPF controller is applied to the PZT actuators. The vibration amplitudes become 0.0485 mm, 0.0163 mm for the set-point control in Fig. 9 and 0.0614 mm, 0.0321 mm for the trajectory tracking control in Fig. 11. It should be noted that the vibration amplitudes in the trajectory tracking control are smaller than those in the set-point control when no PPF strategy. It is expected and reasonable because the smooth reference angle input is used in the trajectory tracking control. From these results, the effectiveness and feasibility of the PPF control algorithm for suppressing multi-mode vibration have been verified.

4.3. Comparison between PPF and velocity feedback

In [16], it was pointed out that the system was unstable if *L*-type velocity feedback law was applied to the PZT actuators located in the middle of the beam. In Section 1,

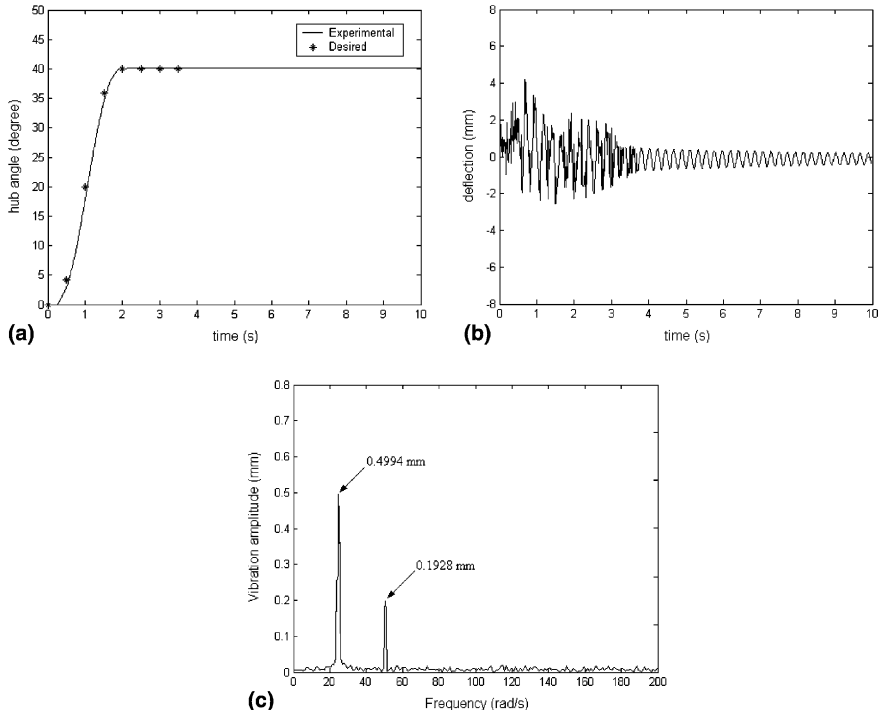

Fig. 10. Trajectory tracking control experiment result without PPF control: (a) Hub angle motion, (b) PSD measurement and (c) FFT of PSD measurement.

we pointed out that one advantage using PPF controller is its insensitive to spillover. In this section, we will verify this by experiments.

Fig. 12 shows the configuration of PZT actuators are boned at the middle of the flexible beam, i.e. $[0.4L, 0.6L]$. For this configuration, the mode parameters will be slightly different from those values listed in Table 2. Experimental results show that the first two vibration frequencies are shifted to be 27.4889 rad/s and 54.1925 rad/s, respectively. This is reasonable because moving the PZT actuators from the tip to the middle will enhance the stiffness of the flexible link.

Fig. 13 shows the experimental result when applying L-type feedback control to the PZT actuators for vibration suppression with 40° set-point slewing. Although the hub angle reaches the desired position (we do not show the plot for hub angle motion), however, the vibration of the flexible beam is excited gradually instead of being suppressed effectively.

Fig. 14 gives the corresponding experimental result when applying PPF control to the PZT actuators at the middle of the beam. The flexible vibration has been suppressed effectively while the slewing is realized. The frequencies for this configuration are used to design the PPF controllers.

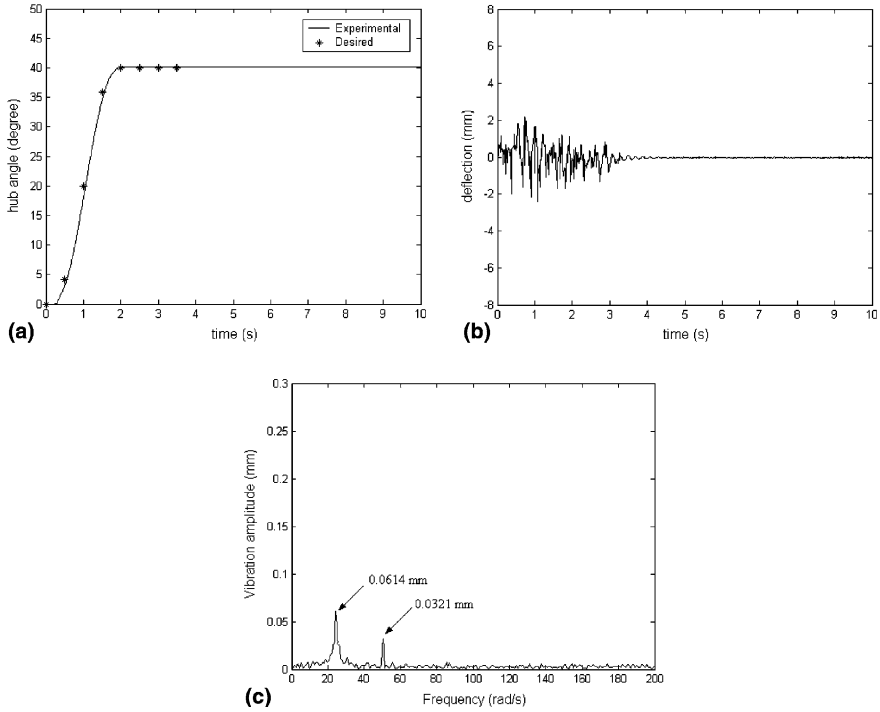

Fig. 11. Trajectory tracking control experiment result with PPF control: (a) Hub angle motion, (b) PSD measurement and (c) FFT of PSD measurement.

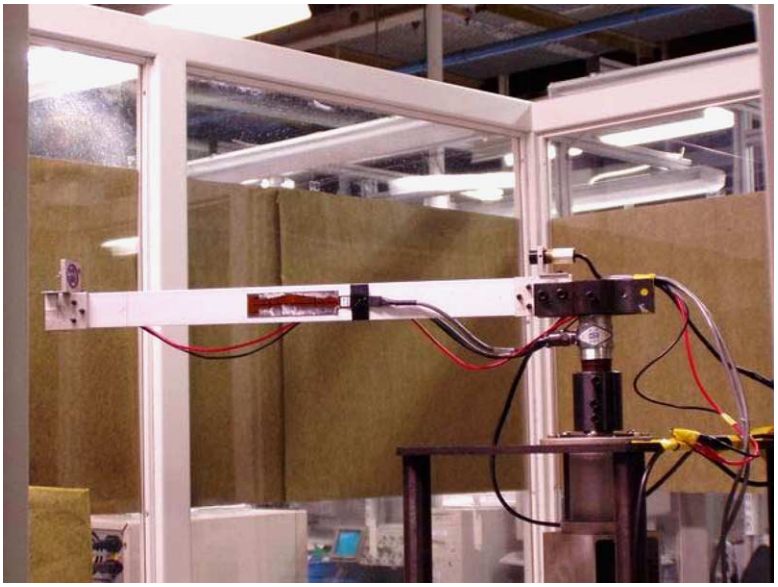

Fig. 12. Photograph of the experimental setup with PZT actuators at the middle.

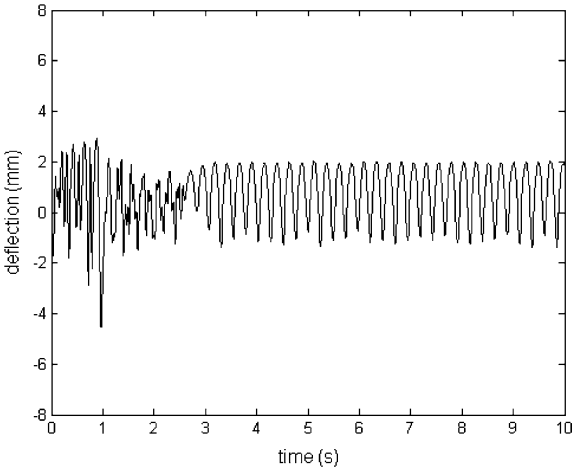

Fig. 13. Experimental result of *L*-type velocity feedback when PZT actuators at the middle.

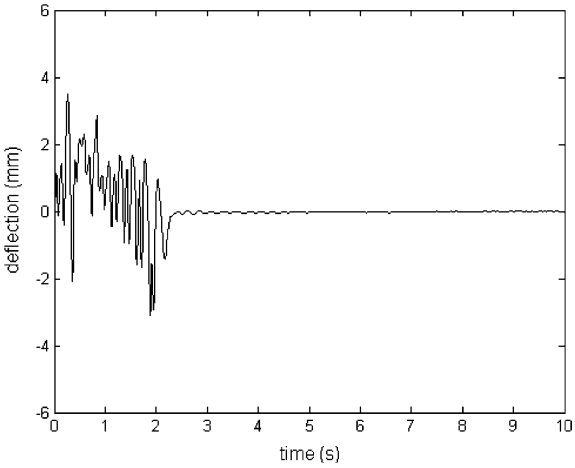

Fig. 14. Experimental result of PPF when PZT actuators at the middle.

5. Conclusions

This paper presents the study on slewing and vibration control of a single-link flexible manipulator using PPF control. The single-link flexible manipulator is bonded with piezoelectric material, PZT, as actuators and uses Position Sensitive Detector (PSD) as sensor. A combined scheme of PD feedback controller for AC servo motor and PPF controller for PZT actuators to suppress multi-mode vibration has been developed and applied to experimental single-link flexible manipulator. For verifying the characteristic of anti-spillover of PPF controller, experiments are

conducted and compared between L-type velocity feedback and PPF strategies for PZT actuators. Experimental results validate the effectiveness of the proposed method.

Acknowledgments

The authors would like to thank the anonymous Reviewers for their valuable comments and suggestions, which significantly improved the quality of this paper.

References

[1] Book WJ. Controlled motion in an elastic world. ASME J Dyn Syst Meas Control 1993;115(1): 252–61.
[2] Moudgal VG, Passino KM, Yurkovich S. Rule-based control for a flexible-link robot. IEEE Trans Control Syst Technol 1994;2(4):392–405.
[3] Singer NC, Seering WP. Preshaping command inputs to reduce system vibration. ASME J Dyn Syst Meas Control 1990;112(1):76–82.
[4] Shan J, Sun D, Liu D. Design for robust component synthesis vibration suppression of flexible spacecrafts with on–off actuators. IEEE Trans Rob Autom 2004;20(3):512–25.
[5] Elahinia MH, Ashrafiuon H. Nonlinear control of a shape memory alloy actuated manipulator. ASME J Vib Acoust 2001;123(4):487–95.
[6] Giurgiutiu V, Jichi F, Berman J, Kamphaus JM. Theoretical and experimental investigation of magnetostrictive composite beams. Smart Mater Struct 2001;10(5):934–45.
[7] Leng J, Asundi A. Active vibration control system of smart structures based on FOS and ER actuator. Smart Mater Struct 1999;8(2):252–6.
[8] Bailey T, Hubbard JE. Distributed piezoelectric-polymer active vibration control of a cantilever beam. J Guidance Control Dyn 1985;8(5):605–11.
[9] Sun D, Mills JK. Control of a rotating cantilever beam using a torque actuator and a distributed piezoelectric polymer actuator. Appl Acoust 2002;63(8):885–99.
[10] Tzou HS, Tseng CI. Distributed piezoelectric sensor/actuator design for dynamic measurement/ control of distributed parameter system: a piezoelectric finite element approach. J Sound Vib 1990; 138(1):17–34.
[11] Choi SB, Shin HC. A hybrid actuator scheme for robust position control of a flexible single-link manipulator. J Rob Syst 1996;13(6):359–70.
[12] Shin HC, Choi SB. Position control of a two-link flexible manipulator featuring piezoelectric actuators and sensors. Mechatronics 2001;11(6):707–29.
[13] Kim Y, Suk JY, Junkins JL. Near-minimum-time slewing and vibration control of smart structures. Structronic systems: smart structures, device & systems, part II. World Scientific Publishing Company; 1998.
[14] Yang SM, Lee YJ. Vibration suppression with optimal sensor/actuator location and feedback gain. Smart Mater Struct 1993;2(4):232–9.
[15] Maxwell ND, Asokanthan SF. Optimally distributed actuator placement and control for a slewing single-link flexible manipulator. Smart Mater Struct 2003;12(2):287–96.
[16] Sun D, Mills JK, Shan JJ, Tso SK. A PZT actuator control of a single-link flexible manipulator based on linear velocity feedback and actuator placement. Mechatronics 2004;14(4):381–401.
[17] Cady WG. Piezoelectricity. New York: Dover; 1964.
[18] Jha R, Rower J. Experimental investigation of active vibration control using neural networks and piezoelectric actuators. Smart Mater Struct 2002;11(1):115–21.
[19] Silva S, Ribeiro R, Rodrigues J, Vaz M, Monteiro J. The application of genetic algorithms for shape control with piezoelectric patches-an experimental comparison. Smart Mater Struct 2004;13(1):220–6.

[20] Ma KG. Vibration control of smart structures with bonded PZT patches: novel adaptive filtering algorithm and hybrid control scheme. Smart Mater Struct 2003;12(3):473–82.
[21] Mayhan P, Washington G. Fuzzy model reference learning control: a new control paradigm for smart structures. Smart Mater Struct 1998;7(6):874–84.
[22] Goh CJ, Caughey TK. On the stability problem caused by finite actuator dynamics in the collocated control of large space structure. Int J Control 1985;41:787–802.
[23] Friswell MI, Inman DJ. The relationship between positive position feedback and output feedback controllers. Smart Mater Struct 1999;8(3):285–91.
[24] McEver MA, Leo DJ. Autonomous vibration suppression using on-line pole-zero identification. ASME J Vib Acoust 2001;123(4):487–95.
[25] Song G, Schmidt SP, Agrawal BN. Experimental robustness study of positive position feedback control for active vibration suppression. J Guidance, Control, Dyn 2002;25(1):179–82.